Chapter 4
Structure and Catalytic Mechanism of β-Carbonic Anhydrases

Roger S. Rowlett

Abstract The β-carbonic anhydrases (β-CAs) are a structurally distinct family of carbonic anhydrase that is widely distributed in microorganisms, algae, plants, and invertebrates. Like all carbonic anhydrases, β-CAs catalyze the reaction $CO_2 + H_2O \leftrightarrows HCO_3^- + H^+$, and is typically associated with other enzymes that produce or utilize CO_2 or HCO_3^-. β-CA is required for normal growth for many organisms. Unique among the five different families of carbonic anhydrases, β-CA is the only family of carbonic anhydrase to exhibit allostery. This chapter summarizes the structure, catalytic mechanism, and allosteric regulation of β-CA.

Keywords Allostery • β-carbonic anhydrases • Ribulose-1, 5-phosphate carboxylase • Crystal structure • Bicarbonate • Catalytic mechanism • Proton transfer • Spinach • Garden pea • Arabidopsis • *E.coli*

1 Introduction

The β-carbonic anhydrases (CAs) were first recognized as an evolutionarily distinct class of carbonic anhydrase in 1990, when the DNA sequence of the gene coding for the enzyme from *Spinacea oleraceae* was obtained [1]. This class of CAs received the β designation because it was the first convergently evolved CA (after α-CA) to have been discovered. Since then, several additional convergently evolved CAs (γ, δ, and ζ) have been discovered. Since the recognition of *S. oleraceae* CA as

Susan C. Frost and Robert McKenna (eds.). Carbonic Anhydrase: Mechanism, Regulation, Links to Disease, and Industrial Applications

R.S. Rowlett (✉)
Department of Chemistry, Colgate University, Hamilton, NY, USA
e-mail: rrowlett@colgate.edu

S.C. Frost and R. McKenna (eds.), *Carbonic Anhydrase: Mechanism, Regulation, Links to Disease, and Industrial Applications*, Subcellular Biochemistry 75,
DOI 10.1007/978-94-007-7359-2_4,

a β-CA, many additional β-CAs—putative and verified—have been discovered, and found to occur in a wide range of organisms, including algae, bacteria, yeast, archaeal species, worms, and insects. Perhaps unlike any other class of CA, β-CAs exhibit a broad structural and functional diversity, including allostery, and the ability to hydrolyze related, alternative substrates, like carbon disulfide. This chapter will focus on the structure and catalytic mechanism of the β-CAs.

2 Distribution and Significance

2.1 Distribution

CA activity was first recognized in plant chloroplasts from *Trifolium pratense* and *Onoclea sensibilis* [2]. Remarkably, plant chloroplast CA was not recognized as a β-CA until more than 50 years later, when the cDNA of the homologous enzymes from spinach (*S. oleraceae*), garden pea (*Pisium sativum*) and *Arabidopsis thaliana* were sequenced [1, 3, 4]. The bulk of what is known about the structure and mechanism of the plant β-CAs has been derived from studies of these three enzymes, which inhabit the chloroplastic stroma. However, additional β-CAs are thought to be localized in the thylakoid space, cytoplasm, and mitochondria of higher plants and algae [5].

The *CynT* gene of *E. coli* was the first recognized β-CA in bacteria. Since that time, many additional bacterial β-CAs have been identified [6–8], including enzymes from well-known human pathogens such as *Mycobacterium tuberculosis*, *Helicobacter pylori* [9], *Salmonella enterica* [10], *Brucella suis* [11], and *Streptococcus pneumoniae* [12]. β-CAs are also found in other microorganisms including the archaea (*Methanobacterium thermoautotrophicum*) [13], yeast (*Saccharomyces cereviseae*) [14], cyanobacteria (*Sychechocystis PCC6803*) [15], chemoautotrophic bacteria (*Halothiobacillus neapolitanus*) [16], and in green (*Chlamydomonas reinhardtii*) [17] and red (*Porphyridium purpureum*) [18] algae.

More recently, β-CAs have been discovered in animal species, including *Drosophila melanogaster* [19] and *Caenorhabditis elegans* [20]. Genomic sequence analysis suggests that β-CAs are widely distributed among non-chordates and invertebrates, but have not yet been demonstrated to exist in any vertebrate species [19].

2.2 Physiological Role and Significance

The physiological role(s) of β-CA are not well-known. However, for those organisms for which there is useful data, β-CA often serves in a support role for enzymes that utilize or dispose of CO_2 or HCO_3^-, such as ribulose-1,5-bisphosphate carboxylase (Rubisco), urease, cyanase, and carboxylases associated with fatty

acid biosynthesis. In *P. sativum*, Rubisco and β-CA are transcriptionally linked and experience an increase in expression levels when plants are transferred from a high CO_2 environment to one with lower, atmospheric pressure of CO_2 [21]. However, it should be noted that tobacco (*Nicotiana tabacum*) plants with antisense suppression of β-CA expression show no clear decrease in carbon assimilation despite having as small as 1 % of normal chloroplastic β-CA levels [22]. β-CA is an essential component of the carboxysome, a CO_2-concentrating structure in cyanobacteria. Mutagenesis of this β-CA results in a phenotype that requires high CO_2 concentrations for normal growth in *Synechococcus* [23]. β-CA has also been determined to be essential for normal growth of *Escherichia coli* [24], *Corynebacterium glutamicum* [25], and *Saccharomyces cerevisiae* [26, 27] under aerobic conditions and atmospheric pressures of CO_2. In β-CA-deficient strains of *S. cerevisiae*, complementation with catalytically competent α- or β-CA restores the ability to grow normally under atmospheric CO_2 concentrations [27]. In β-CA deficient *Streptococcus pneumoniae*, complementation with unsaturated fatty acids restores normal growth under low CO_2 concentration conditions [28]. This suggests that β-CA in this organism, and perhaps in other bacteria and yeast, supports the activity of bicarbonate-dependent carboxylases required for fatty acid synthesis. *Helicobacter pylori* has both α- and β-CA gene, which are localized to the periplasm and cytoplasm, respectively. Deletion of the α-CA affects CO_2-HCO_3^- exchange rates and delays the urease-dependent increase in extracellular pH in *H. pylori*, whereas deletion of β-CA does not. However, β-CA deficient *H. pylori* produced strongly reduced gastric mucosal inflammation in mouse models of *H. pylori* infection [29].

In animal species, the physiological roles of β-CA are not established. The *Drosophila melanogaster* β-CA is localized to the mitochondrion, and is possibly involved in gluconeogenesis, ureagenesis, and/or lipogenesis, but this has not been directly demonstrated [19]. In *C. elegans,* no observable phenotype was observed for RNAi suppression of β-CA expression [20].

Finally, some β-CAs have adapted evolved to adopt novel metabolic functions. The *Acidianus* carbon disulfide hydrolase is clearly structurally and genetically closely related to β-CA. This enzyme cleaves CS_2 to COS and H_2S, but has no detectable CO_2 hydration activity [30].

3 Structure

The first X-ray crystallographic structures of β-CA were not determined until 2000, nearly a decade after the discovery of β-CA as an evolutionarily distinct class of CA. The first β-CA structure to be determined was for the red alga *P. purpureum* [18]. Structures for the *P. sativum* [31] and *E. coli* [32] enzymes followed quickly. As of this writing, there are a total of 12 distinct X-ray crystallographic structures of β-CAs deposited in the Protein Data Bank (Table 4.1).

Table 4.1 Structurally and kinetically characterized β-CAs

Source	PDB entry	Abbreviation	Structural subtype[a]
Pisium sativum	1EKJ	PSCA	Type I
Spinacea oleraceae	—	SOCA	Type I
Arabidopsis thaliana	—	ATCA	Type I
Methanobacterium thermoautotrophicum	1G5C	MTCA	Type I
Mycobacterium tuberculosis Rv1284	1YLK	Rv1284	Type I
Halothiobacillus neopolitanus	2FGY	HNCA	Type I
Coccomyxa	3UCO	CoCA	Type I
Saccharomyces cerevisiae	3EYX	SCCA	Type I
Streptococcus mutans	3LAS	SMCA	Type I
Porphyridium purpureum	1DDZ	PPCA	Type II
Escherichia coli	1I6P	ECCA	Type II
Haemophilus influenzae	2A8D	HICA	Type II
Mycobacterium tuberculosis Rv3588	1YM3	Rv3588	Type II
Salmonella enterica	3QY1	SECA	Type II

[a]Structural subtypes are described in Sect. 3.5

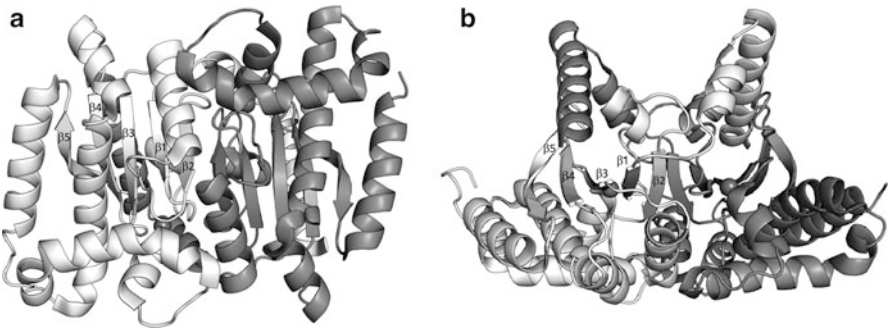

Fig. 4.1 Fundamental dimer of HICA. *Panel B* is rotated 90° about its horizontal axis relative to *panel A*. Monomers are colored *white* and *gray*. The dimerization interface lies along the *vertical axis* of panels *A* and *B*. The tetramerization interface lies along the face of *panel A* and the bottom of *panel B* (see Sect. 3.3)

3.1 β-CAs Are Composed of Dimers

The β-CAs are characterized by a unique α/β fold that associates to form dimers. In some β-CAs, this basic structural dimer is a single polypeptide chain composed of a tandem repeat of the a monomer sequence connected by a short polypeptide linker—a "pseudo-dimer." The β-CA monomer (or pseudo-monomer) is composed of a central core formed from a four-strand parallel β-sheet in a 2-1-3-4 arrangement (Fig. 4.1). Some β-CAs incorporate a short fifth β-strand that associates with β4 in an antiparallel arrangement. In most β-CAs the β-sheet cores of the fundamental structural dimer or pseudo-dimer are associated in an approximately antiparallel arrangement to form an 8–10 strand β-sheet that extends across the entire assembly.

More than a half-dozen α-helices pack against the β-sheet core, and with β5, when present, form the solvent-accessible surface of the dimer or pseudo-dimer unit. The fundamental dimer of β-CA is a tightly integrated structure. There are extensive interactions between monomer units in the region where the two β-sheet cores contact each other. In addition, two N-terminal helices wrap around the neighboring monomer like a clasp, where α1 of one monomer interacts with β4 and β5 from the neighboring monomer. For most β-CAs the total buried surface area [33] of the dimerization interface is approximately 7,000 $Å^2$, or 3,500 $Å^2$ per monomer unit.

HNCA departs significantly from the canonical dimer structure of β-CA. This β-CA is composed of three distinct domains: an N-terminal four-helix bundle; a catalytic domain that is similar to that of other β-CA monomers in structure; and a C-terminal domain that is similar in structure to the catalytic domain, but has lost its catalytic site, including metal ion binding residues [16]. This enzyme is so structurally distinct from other β-CAs that is was originally thought to be a member of a distinct (ε) family of CA, but is now recognized as a variant of β-CA [34].

The *Acidanius* carbon disulfide hydrolase (PDB 3TEN) is also very likely a divergently evolved β-CA [30]. It shares the same 2-1-3-4 central β-sheet core structure and dimer organization as β-CA, with 1.55 Å rmsd 3D structural homology over 70 % of the aligned sequence to *M. thermotautotrophicum* β-CA.

3.2 β-CAs Are Zinc Metalloenzymes

With one exception—HNCA, which is missing one active site—all β-CAs that have been structurally characterized contain one zinc ion per monomer or pseudo-monomer. The metal ion is in a pseudo-tetrahedral $Cys_2His(X)$ coordination environment where X is either an Asp residue or an exchangeable ligand such as water or an inorganic or organic anion. The zinc ion is the location of the catalytic (active) site. The pseudo-dimer of HNCA is asymmetric. In this enzyme, one of the pseudo-monomers has lost its metal-binding site during the course of evolution [16].

3.3 Quaternary Structure of β-CAs

The biological units of β-CAs are multiples of the fundamental dimer structure. Dimers, tetramers, and octamers are known or suggested from X-ray crystallographic data (Fig. 4.2).

3.3.1 Tetramers

The most frequently observed quaternary structure for β-CA is a tetramer. HICA, ECCA, COCA, SCCA, Rv1284 and SECA adopt a homotetrameric structure based on interface analysis of the X-ray crystal structures [33], and this has been verified

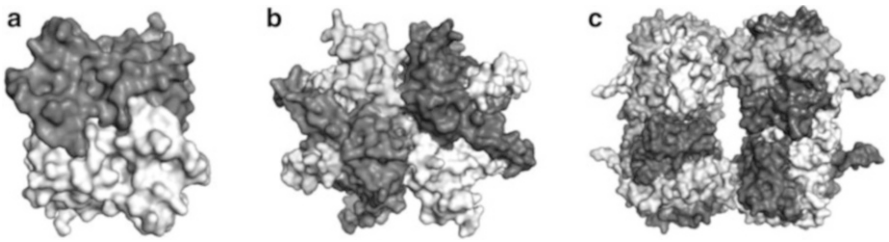

Fig. 4.2 Quaternary structures of β-CAs. (**a**) Rv3588 dimer. Dimerization interface is horizontal. (**b**) HICA tetramer. Dimerization interface is *horizontal*; tetramerization interface is *vertical*. (**c**) PSCA octamer. The tetramerization interfaces are along the *horizontal axis*; the octamerization interfaces are along the *vertical axis*

by gel exclusion chromatography for HICA [35]. PPCA [18] and HNCA [16] adopt analogous pseudo-tetrameric structures by the association of their pseudo-dimers. β-CA tetramers are best described as a dimer of dimers with 222 symmetry and two distinct oligomerization interfaces, one of which—the "dimerization" interface—has been described previously. The "tetramerization" interface is primarily composed of α-helices that form a nearly flat face on the fundamental dimer (Fig. 4.1). The total buried surface area [33] at the tetramerization interface is about 1,600–1,700 $Å^2$ for HICA, ECCA, STCA, and Rv1284, and similar values are obtained for the association of pseudo-dimers for HNCA. Thus it appears that the tetramerization interaction is perhaps only a quarter or a third as strong as the dimerization interface. The tetramerization interface of PPCA and COCA is significantly larger than the other tetrameric or pseudo-tetrameric β-CAs with a total buried surface area of ≈4,700 $Å^2$ and 3,500 $Å^2$, respectively. MTCA forms crystals in which there is no reasonable tetramerization interface in the asymmetric unit [36]. MTCA is missing most of the N- and C-terminal helices that characterize most of the other β-CAs. In particular, MTCA is missing both α1 and α2, structural features that are typically integral to the dimerization interface; instead, residues 90–125 form a pair of helices (α4 and α5) that fulfill this role. The location of helices α4 and α5 on the tetramerization interface appears to preclude tetramerization of this enzyme in the same manner as HICA or its homologs. However, gel exclusion chromatography [13] and analytical ultracentrifugation [37] suggest that the MTCA exists in solution as a tetramer. The crystal structure of MTCA has an unusual, but probably artifactual feature where the N-terminal helix of chain A appears to be domain swapped with its nearest crystal-packing neighbor, where it packs against β4 and β5, similar to that of tetrameric β-CAs. It seems likely that in vitro the N-terminal helix of chain A of MTCA is arranged similarly to that of chain B.

3.3.2 Dimers

Native Rv3588 forms crystals that contain a single monomer per asymmetric unit in a manner that can allow for the formation of a dimer, but not a tetramer with

symmetry partners in the unit cell [38]. The thiocyanate complex of the same enzyme crystallizes with a dimer-of-dimers homotetramer in the asymmetric unit [39]. Dynamic light scattering studies show that the enzyme exists primarily as a tetramer at high pH, and dissociates into dimers when the pH is lowered from 8.4 to 7.5. Unlike other tetrameric β-CAs, Rv3588 has a high concentration of basic residues in the tetramerization interface that participate in salt bridges that stabilize the dimer-dimer interaction. Basic residues outnumber acidic residues in the tetramerization interface by almost two to one. It seems likely that high pH is required for tetramerization in order to neutralize excess positive charge at the tetramerization interface [39].

The *Drosophila melanogaster* β-CA has been characterized by gel exclusion chromatography and by dynamic light scattering, and suggest that it exists as a dimer in vitro [19].

3.3.3 Octamers

The biological unit of PSCA is an octamer with 222 symmetry: a dimer of a dimer of dimers [31]. The structural feature that is likely responsible for this organization is an extended C-terminus that forms a long β5 strand which engages in an antiparallel β5-β5′ interaction that allows dimers to associate into higher-order quaternary structures. The assembly of the PCSA octamer involves a "tetramerization" interface of ≈1,700 Å^2 total interaction area, and an "octamerization" interface with a total contacts area of ≈1,500 Å^2 [31]. The resulting structure looks something like a square ring. Gel exclusion chromatography studies of SOCA [40] and non-denaturing gel electrophoresis of SOCA and ATCA [41] are consistent with an octameric quaternary structure for these homologous enzymes.

The *Acidianus* carbon disulfide hydrolase adopts a quaternary structure remarkably like PSCA. However, in the case of the *Acidianus* enzyme, two octameric rings appear to interlock to form an unusual hexadodecameric catenane. Analytical ultracentrifugation and small angle X-ray scattering confirm the expected molecular weight of the catenane structure [30].

3.4 Post-translational Modification of Plant β-CAs

The genes that code for the precursor of chloroplast β-CAs contain a Ser/Thr rich chloroplastic transit peptide [1, 42–45]. Native SOCA and PSCA isolated from plants suggests that processing of the transit peptide is heterogeneous. In particular PSCA appears to exist as two discrete molecular weight forms [45] resulting from the proteolysis of the transit peptide in two sequential steps [46]. These different forms of PSCA do not appear to differ significantly in catalytic activity [45].

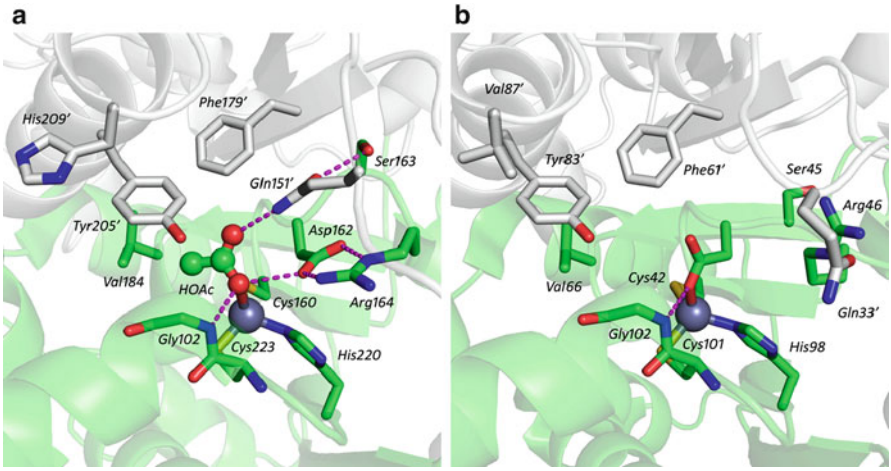

Fig. 4.3 Active site regions of archetypical Type I (PSCA, PDB 1EKJ chains G & H, *panel A*) and Type II (HICA, PDB 2A8D chains D & F, *panel B*) β-CAs. The active site monomer is *green*; the neighboring protein chain in the fundamental dimer is *gray*. Zinc is depicted as a *gray sphere*. Key residues, including acetic acid (HOAc) are depicted as *sticks* and/or *spheres*. *Dashed magenta lines* indicate hydrogen bonding interactions

3.5 Two Classes of β-CA Are Defined by Active Site Structure

X-ray crystallography of β-CAs reveal two distinct structural subclasses differentiated by the nature of the fourth metal ion ligand and a characteristic triad of residues (Trp, Tyr, and Arg) in a putative allosteric site. These two classes of β-CA—Type I and Type II—are not defined by genetic origins, but rather by active site organization and functional behavior (*vide infra*). The type classification of structurally and functionally well-characterized β-CAs is listed in Table 4.1.

3.5.1 Type I (Open) β-CAs

Type I β-CAs are characterized by three principal structural features. The first is a $Zn(Cys)_2(His)(X)$ coordination sphere in which X is an exchangeable ligand, such as water or an inorganic or organic ion. In active enzyme this fourth ligand is assumed to be a water or hydroxide ion. The second structural feature is an Asp-Arg dyad in which the Asp residue acts as a hydrogen bond acceptor from water, hydroxide, or an OH or NH group that is ligated to the metal ion. The third is a hydrogen bond donor (typically a Gln or His) that can interact with a distal oxygen of metal ion bound bicarbonate or bicarbonate analog. The defining example of a Type I β-CA is PSCA (Fig. 4.3a). The active site metal ion, as in all β-CAs, is situated on the dimerization interface. In PSCA the exchangeable ligand is acetic acid, a bicarbonate analog. In this structure, Arg164 stabilizes and orients Asp162

so that it can accept a hydrogen bond from the OH group of the bound acetic acid. Asp162 is hypothesized to act as a "gate-keeper" residue, excluding anions or other ligands from the metal ion that cannot donate a hydrogen bond from the metal-bonded atom. Gln151′ from the neighboring monomer donates a hydrogen bond to the distal oxygen atom of acetic acid. Finally, the amide NH of Gly224 donates a hydrogen bond to the proximal, metal-bound oxygen atom of acetic acid. The binding of acetic acid to PSCA is probably representative of the enzyme-bicarbonate intermediate in catalysis.

The active site tunnel leading to the metal ions lies along the dimerization interface and is highly constricted. It is lined with hydrophobic residues: Phe 179′, Val184, and Tyr205′ in PSCA. The only polar residue in the active site cleft is His209′, which lies at the exterior surface of the active site opening. For most β-CAs that have been structurally characterized by X-ray crystallography, the active site opening is too small to accommodate CO_2 or HCO_3^-. Therefore, there must be considerable rearrangement of the bulky side chains to allow for substrate/product ingress/egress.

The active site of PSCA is a remarkable example of convergent evolution: it maps nearly perfectly on a mirror image of the active site of human α-CA II (HCAII) [31], a CA whose mechanism of action is well understood. The mapping of analogous residues/atoms in PSCA onto HCAII allow the designation of catalytic roles of functional groups in β-CA. The most significant mappings include Asp162-Oδ1 in PSCA and Thr199-Oγ1 in HCAII. In HCAII, Thr199-Oγ1 donates a hydrogen bond to the side chain of Glu106, so that Thr199 is an obligate hydrogen bond acceptor from the atom bound to the metal ion. That is, Thr199 acts as the "gatekeeper" residue in HCAII, and by analogy, so does Asp162 in PSCA. The main chain amide of Thr199 in HCAII is hypothesized to donate a hydrogen bond to the distal oxygen atom of bicarbonate curing catalysis; in PSCA, the amide group of Gln151′ plays an analogous role. Notably, both Asp162 and Gln 151 (PSCA numbering) are highly conserved in β-CAs.

The carboxysomal enzyme HNCA possesses an active site similar to Type I β-CAs, but this enzyme is somewhat of an anomaly. It has only 15 % sequence identity with other β-CAs and has numerous insertions and deletions compared to the typical β-CA. Most significantly, the active site has been entirely lost from one of the pseudo-dimers. Both HNCA and Rv1284 utilize a His residue in place of the analogous Gln151′ in PSCA.

3.5.2 Type II (Closed) β-CAs

HICA is the archetype for Type II β-CAs (Fig. 4.3b). Type II β-CAs have a closed $Cys_2HisAsp$ coordination sphere around the active site metal ion, and significant changes in other structural features that characterize Type I β-CAs (Fig. 4.3b). Specifically, the Asp-Arg dyad of Type I β-CAs is broken, and the hydrogen bond donor residue (Gln151′ in PSCA, Gln33′ in HICA) is rotated away from the active site. In PSCA, Ser163 donates a hydrogen bond to the side-chain carbonyl of

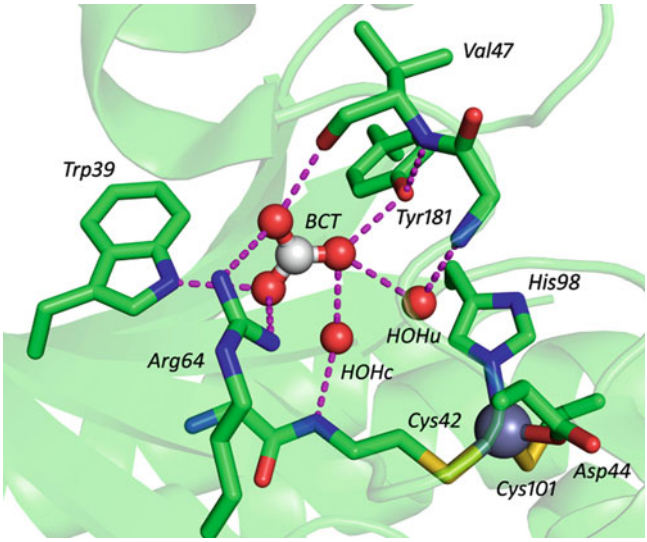

Fig. 4.4 Non-catalytic (allosteric) bicarbonate binding site in HICA (PDB 2A8D, chain D). Key residues, including bicarbonate (BCT) and the common and unique water molecules (HOHc and HOHu, respectively) are depicted as *sticks* and/or *spheres*

Gln151′, orienting it properly to donate a hydrogen bond to the distal oxygen of metal-bound acetic acid or bicarbonate. In HICA, the analogous Ser45-Gln33′ interaction is broken because the 44–48 loop has been rotated about 90° relative to the comparable region in PSCA.

Some type II β-CAs also have a non-catalytic bicarbonate binding site (Fig. 4.4) characterized by a Trp-Arg-Tyr triad (Trp39, Arg64, and Tyr181 in HICA). The non-catalytic binding site has been characterized by X-ray crystallography for ECCA and HICA [35]. It is located near the dimerization interface, opposite the tetramerization interface. A network of 7 highly specific hydrogen bonds serves to bind the bicarbonate in this site. The indole nitrogen of Trp39, two of the guanidinium NH groups of Arg64, the hydroxyl group of Tyr181, and two water molecules donate hydrogen bonds to the oxygen atoms of bicarbonate. One of these water molecules is found in many Type I and Type II β-CAs. This water accepts a hydrogen bond from the main-chain amide of Cys42. The other water molecule is unique to HICA and ECCA. It is positioned ≈3.4 Å directly above the imidazole ring of His98, where it can engage in a π-hydrogen bond, and accept a hydrogen bond from the main chain amide of Arg46. A final hydrogen bond exists between the main-chain carbonyl of Val47 and the hydroxyl group of bicarbonate. This is the only hydrogen bonding interaction in the binding site in which bicarbonate ion acts as a donor. This arrangement of hydrogen bonds is quite specific for bicarbonate: isolectronic anions such as nitrate or acetate are not able to act as a donor to the Val47 main-chain carbonyl. While HICA crystals soaked in bicarbonate ion

readily bind it into the non-catalytic site, identical crystals soaked in up to 1 M acetate or nitrate are not observed to bind these ions in the bicarbonate binding site (R. Rowlett, unpublished results).

Binding of bicarbonate to the non-catalytic site stabilizes the conformation of the 44–48 loop that characterizes the structure of Type II β-CAs. The binding of the bicarbonate ion to the non-catalytic site expels the side chain of Val47, which causes a reorganization of the Asp44-Pro48 loop. This reorganization apparently breaks the Asp44-Arg46 dyad, which in turn allows Asp44 to bind directly to the metal ion, displacing the catalytically essential water molecule. Additionally, the rotation of the Asp44-Pro48 loop repositions Ser45 so that it can no longer stabilize Gln33′ in an orientation favorable for stabilizing the binding of an anionic ligand to the metal ion. The noncatalytic bicarbonate binding site is thought to mediate allosteric behavior in Type II β-CA (*vide infra*).

While the existence of the non-catalytic binding site has been shown only for HICA and ECCA, it is likely that many other type II β-CAs can bind bicarbonate in this fashion as well. SECA and PPCA have an identical triad, whereas Rv3588 substitutes an Ile residue for the Trp. SMCA, although it is classified as a Type II β-CA here, is missing most of the non-catalytic bicarbonate binding groups: it has a Val residue instead of Trp, and does not have the equivalent of Tyr181 in HICA because of a truncated C-terminus. All structurally characterized Type I β-CAs are missing one or more elements of the Trp-Arg-Tyr triad that characterizes the non-catalytic bicarbonate binding site.

4 Catalytic Mechanism

SOCA, PSCA, ATCA, MTCA, and HICA have been thoroughly kinetically characterized. Measurements of the rate of CO_2 hydration at steady state by stopped-flow spectrophotometry shows that β-CAs, like other CAs, are very fast enzymes with maximal k_{cat} values as high as 950 ms^{-1} and k_{cat}/K_m values as high as 180 $\mu M^{-1}\ s^{-1}$ (Table 4.2). MTCA and HICA are significantly slower enzymes than the eukaryotic enzymes.

The catalytic mechanism of β-CA follows a metal-hydroxide mechanism similar to that of other CAs (Fig. 4.5). This assessment is based on the close structural homology of the β-CA and α-CA active sites [31], as well as a wealth of kinetic evidence. Among the most convincing data is that β-CAs catalyze the exchange of O-18 in isotopically labeled bicarbonate in a way that can only be rationalized by deposition of the O-18 label at the active site metal ion during catalysis [35, 41, 47].

In the first step of the mechanism for CO_2 hydration, CO_2 is concentrated in the active site by association with a number of hydrophobic residues that line the active site cleft. CO_2 is known to bind to a similar hydrophobic pocket in the active site of HCAII [52]. This trapped CO_2 is then attacked by the zinc-bound hydroxide ion (step A → B in Fig. 4.5), the active species of the enzyme for CO_2 hydration. The hydroxide ion is properly oriented by the Asp-Arg dyad and the main chain

Table 4.2 Steady state kinetic parameters for CO_2 hydration for selected β-CAs

Enzyme	k_{cat} (ms^{-1})	k_{cat}/K_m ($\mu M^{-1}\ s^{-1}$)
SOCA[a]	163 ± 1	—
PSCA[b]	400	180
ATCA[c]	320 ± 20	68 ± 11
MTCA[d]	24 ± 2	8.3 ± 0.7
HICA[e]	69 ± 29	4.3 ± 0.8
SCCA[f]	940	98
DMCA[g]	950	110

[a]Maximal values at high pH [47]
[b]Values at pH 9.0 [48, 49]
[c]Maximal values at high pH [41]
[d]Values at pH 8.5 [37, 50]
[e]Maximal values at high pH [35]
[f]Values at pH 8.3 [51]
[g]*Drosophila melanogaster* enzyme; values at pH 8.3 [19]

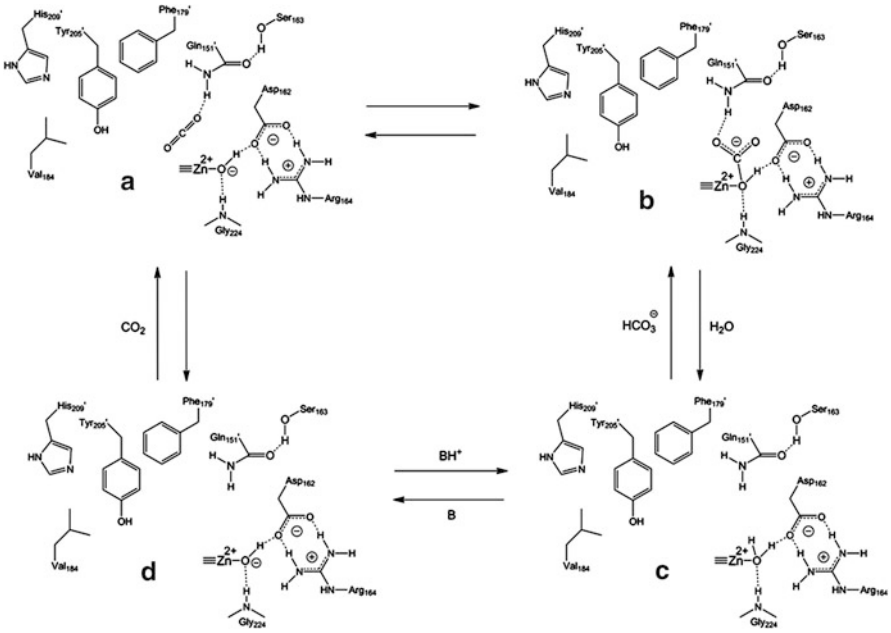

Fig. 4.5 Catalytic Mechanism of β-CA. Residue numbering system is for PSCA. "B" represents an external hydrogen ion acceptor; "BH^+" represents an external hydrogen ion donor. CO_2 hydration is represented by D-A-B-C-D; HCO_3^- dehydration proceeds as C-B-A-D-C. Figure adapted from [8]

amide of the active site Gly for nucleophilic attack of CO_2. The developing negative charge on the metal-bound bicarbonate ion is partly neutralized by hydrogen bond donation from the side chain amide of a Gln (His in MTCA and HTCA) from the neighboring subunit. In the third step of the mechanism (B → C in Fig. 4.5) water

exchanges for bicarbonate at the metal ion, completing the conversion of CO_2 to HCO_3^-. To regenerate the original, active form of the enzyme, a hydrogen ion must be lost (C → D in Fig. 4.5). The final acceptor of this hydrogen ion are exogenous buffer molecules. However, it seems likely that one or more proton shuttle residues (PSRs) are involved, considering the distance (≈8–10 Å) between the metal-bound water molecule and the surface of the protein. Site-directed mutagenesis suggests that the active site His and Tyr residues (209 and 212 in PSCA) are important for proton transfer in PSCA [53] and ATCA [41]. In MTCA, the active site Asp34 residue has a role in proton transport as well [50]. Although it has not been experimentally tested, in the non-plant β-CAs the weakly conserved active site Tyr residue (Tyr83 in HICA) is the only polar group in the active site cleft that could act as a PSR. The equivalent of Tyr83 is missing in HTCA, MTCA, and Rv1284, and these β-CAs do not have any other likely candidates for a PSR. This is a likely reason why MTCA is among the slowest of β-CAs.

4.1 Proton Transfer Is the Rate-Determining Step in Catalysis

A significant body of evidence suggests that the rate-determining step for β-CA is the proton transfer step. NMR measurements of the rate of CO_2-HCO_3^- exchange (all steps except C ⇆ D in Fig. 4.5) catalyzed by SOCA show that it is ≈10× faster than the overall rate of catalysis [47]. O-18 isotope exchange experiments conducted with ATCA show that R_1, the rate of CO_2-HCO_3^- exchange at chemical equilibrium, is faster than $R_{H2O,}$ the rate of release of O-18 labeled water from the enzyme [41]. The chemical step measured by the rate R_{H2O} requires the transfer of a proton from an exogenous or endogenous donor to the metal-bound hydroxide ion during the conversion of HCO_3^- to CO_2. For SOCA, PSCA, and MTCA, there is a significant solvent deuterium isotope effect (SDIE) of approximately 2 on k_{cat} for the CO_2 hydration reaction, which strongly suggests that there is a rate-determining hydrogen ion transfer in the mechanism. Additionally, the SDIE for $k_{cat}/K_{m,}$ which includes all steps in Fig. 4.5 except C ⇆ D, is near unity: this means that the origin of the SDIE must reside in step C ⇆ D in Fig. 4.5, i.e., within an intermolecular or intramolecular proton transfer step. The observation that k_{cat} for CO_2 hydration in SOCA [47], PSCA [49], ATCA [41], and MTCA [37], depends upon exogenous buffer concentration in a saturable way suggests that intermolecular proton transfer is rate-limiting at low buffer concentrations, and that an intramolecular proton transfer step may be rate-limiting at high buffer concentrations. This is directly analogous to other classes of CA.

4.2 pH-rate Profiles

Both k_{cat} and k_{cat}/K_m increase with increasing pH for β-CA catalyzed CO_2 hydration [35, 37, 41, 47, 48]. This observation is entirely consistent with the mechanism of

Fig. 4.5. If intramolecular proton transfer is rate-limiting, as it is expected to be at high exogenous buffer concentrations, the pH profile of k_{cat} should be proportional to the fraction of the PSR that is in its conjugate base form. Thus the pH-rate profile of k_{cat} should provide an estimate of the macroscopic pK_a of the PSR. The pH-rate profile of k_{cat}/K_m, on the other hand, should reflect the ionization state of the metal-bound water: specifically k_{cat}/K_m should track with the relative fraction of the metal-hydroxide species present.

The pH-rate profiles of β-CA catalyzed CO_2 hydration are complex, and are likely involve the ionization of more than one species [37, 41, 48]. In addition, non-Michaelis-Menten kinetics are often observed [41, 48]. For ATCA, the pH-rate profile for k_{cat}/K_m can be satisfactorily modeled by a single ionization event with a pK_a of 7.2 ± 0.1 [41]. The H209A variant of PSCA also has a tractable pH-rate profile for k_{cat}/K_m that can be fit to a titration curve with a pK_a of 7.1 ± 0.1 [53]. These studies suggest that the pK_a for the zinc-bound water molecule is near neutrality for plant β-CAs, and is similar to the pK_a of the metal-bound water in α-CAs. This result is somewhat surprising, given the much more electron-rich ligation sphere for the metal ion in β-CA compared to α-CA. The pH-rate profile of k_{cat}/K_m for HICA is highly cooperative, but is estimated to be 7.74 ± 0.04 [35]. This is significantly higher than for plant β-CAs. The pH-rate profiles of k_{cat} are complex for all β-CAs studied so far. In ATCA, it is possible to identify two separate apparent pK_a values of 6.0 ± 0.8 and 8.8 ± 0.3 in the k_{cat} pH profiles [41]. This suggests that there may be two PSRs in plant CAs. Likely candidates are His209 and Tyr 205 (PSCA numbering).

4.3 Site-Directed Mutagenesis Studies

A significant number of site-directed mutagenesis studies have critically examined the mechanism of Fig. 4.5. To date, these studies have been supportive of this mechanism.

4.3.1 Active Site Variants

The role of the active site Gln residue was studied in the Q158A variant of ATCA [54]. Computational studies predict it is important in stabilizing developing negative charge on the metal-bound bicarbonate ion during catalysis [55]. This variant has a k_{cat}/K_m for CO_2 hydration that 33 % of wild type, and a maximal value of R_1/[E] that is an order of magnitude lower than the wild-type enzyme. The k_{cat} for CO_2 hydration and R_{H2O}/[E] values are not significantly altered by this variant. This result strongly suggests that the active site Gln residue is important for catalytic steps involved in the interconversion of CO_2 and HCO_3^-, but not for proton transfer, a result that is consistent with the proposed role for this residue.

The role of the Asp-Arg dyad in β-CA has also been studied. Computational studies suggest that the Asp-Arg dyad is essential for efficient catalysis by orienting the metal bound-hydroxide for nucleophilic attack [55]. The D34A variant of MTCA [50] reduces k_{cat} for CO_2 hydration by an order of magnitude in MOPS buffer, but not at all in the presence of imidazole buffer, suggesting that imidazole can chemically rescue this variant. The rate constant k_{cat}/K_m is relatively unaffected by the mutation of Asp34 to Ala. This observation suggests that the active site Asp residue may play an essential role in proton transfer. However, the replacement of the analogous Asp residue in SOCA [56] or in HICA [57] results in the nearly total loss of activity. Imidazole rescue of SOCA restores only 9 % of its activity at pH 8.0 [56]. All of these results taken together suggest that the dyad Asp residue may play important roles in both CO_2-HCO_3^- conversion and proton transfer. The replacement of Arg36 in MTCA results in the reduction of both k_{cat} and k_{cat}/K_m for CO_2 hydration to 0.1–1.0 % of wild-type [50]. This variant can be partially chemically rescued by exogenous guanidine. This result is consistent with the proposed role of the dyad Arg residue in orienting the dyad Asp residue to orient the metal-bound hydroxide for nucleophilic attack of CO_2.

4.3.2 Proton Transfer Variants

PSRs appear to be a general feature of all CAs, providing an efficient route for proton transfer from the metal-bound water molecule to exogenous proton acceptors. His64 fulfills this role in α-CA [58]; in γ-CA Glu84 performs this role [59]. Likely PSR candidates for β-CA are a highly conserved active site tyrosine residue (Tyr205 in PSCA; Tyr83 in HICA), and a histidine residue that is present in some plant β-CAs (His209 in PSCA), including PSCA, ATCA, and SOCA. The pH-rate profiles of k_{cat} for CO_2 hydration for ATCA suggests that there are two residues that participate in intramolecular proton transfer with apparent pK_a values of approximately 6.0 and 8.8 [41]. The ATCA variant H216N has a pH-rate profile of k_{cat} for CO_2 hydration, and a pH-rate profile of R_{H2O}/[E] that is significantly decreased at low pH, suggesting a role for His216 in proton transfer in this enzyme [41]. The H209A variant of PSCA behaves similarly: the pH-rate profile of k_{cat} for CO_2 hydration is significantly decreased at low, but not high pH [53]. The role of His216 as a PSR in ATCA is strongly supported by the chemical rescue of k_{cat} and R_{H2O}/[E] by exogenous imidazole [41, 60]. The role of the active site tyrosine residue as a PSR is less clear, but the Y212A variant of ATCA has a significantly diminished k_{cat} value at high pH (but not a low pH) compared to the wild-type enzyme [41].

4.4 Metallosubstitution of β-CA

Co(II)-substituted HICA (Co-HICA) can be made by overexpression of this enzyme in zinc-depleted, cobalt(II)-enriched defined growth medium [61]. Co-HICA is a

bright blue color. Like most zinc-metalloenzymes, Co-HICA has catalytic activity very similar to the wild type enzyme, with a maximal k_{cat} of 120 % of the zinc enzyme. The apparent pK_a of the metal-bound water, derived from measurements of the pH-rate profile of k_{cat}/K_m for CO_2 hydration, is 7.48 ± 0.03, similar to or slightly lower than the pK_a of the metal-bound water in the zinc enzyme (7.7 ± 0.4). The visible absorption spectrum of Co-HICA at pH 8.0 is similar to that of other Co(II)-substituted CAs with *d-d* absorption bands at 560 nm ($\varepsilon = 340\ M^{-1}\ cm^{-1}$), 620 nm ($\varepsilon = 720\ M^{-1}\ cm^{-1}$), and 703 nm ($\varepsilon = 290\ M^{-1}\ cm^{-1}$), the last of which may be two overlapping features. The molar absorptivity of these bands increase markedly in a highly cooperative fashion as the pH is lowered, and there is no isosbestic point, suggesting that there than two metal coordination species present. The most likely coordination environments involved are $Co(Cys)_2(His)(Asp44)$, $Co(Cys)_2(His)OH_2$, and $Co(Cys)_2OH^-$ species, with the first predominant at low pH, the last predominant at high pH, and the middle species mixing in at intermediate pH values.

4.5 Inhibitors of β-CA

Like other CAs, β-CAs are inhibited by monovalent anions and sulfonamides [47, 48, 51, 62–68]. The mode of inhibition is probably similar to that of other CAs: that is, anions and sulfonamides (in the deprotonated anionic form) bind to the active site zinc ion, displacing the catalytically essential water molecule. Direct evidence for anion binding to β-CA comes from the X-ray crystal structure of the thiocyanate complex of Rv3588, in which the nitrogen atom of thiocyanate is observed to be directly bound to the zinc ion in place of the catalytic water [39]. The affinity of inhibitors varies greatly between various CAs, but in general, anions and sulfonamides inhibit plant β-CAs more strongly than for microbial β-CAs [8]. Plant β-CAs have anion K_i values that are comparable to that of α-CAs, but for MTCA similar anion K_i values are 1–2 orders of magnitude higher. In α-CA, acetazolamide and ethoxzolamide are potent inhibitors with K_i values in the nanomolar to picomolar range [69]. For PSCA and MTCA, these inhibitors have K_i values in the micromolar range. Phenylboronic and phenylarsonic acids are more potent inhibitors of MTCA β-CA than α-CA, with K_i values in the micromolar range [70]; these inhibitors are moderately specific for β-CA relative to α-CA.

5 Allostery

Another defining characteristic of type II β-CAs are dramatically steep pH-rate profiles. ECCA and HICA [35], SECA [10], and Rv3588 [38] all show a sudden loss of enzymatic activity below pH 8.0. pH-rate profiles of k_{cat} and $R_{H2O}/[E]$ for HICA-catalyzed CO_2 hydration show highly cooperative behavior that correlates to the

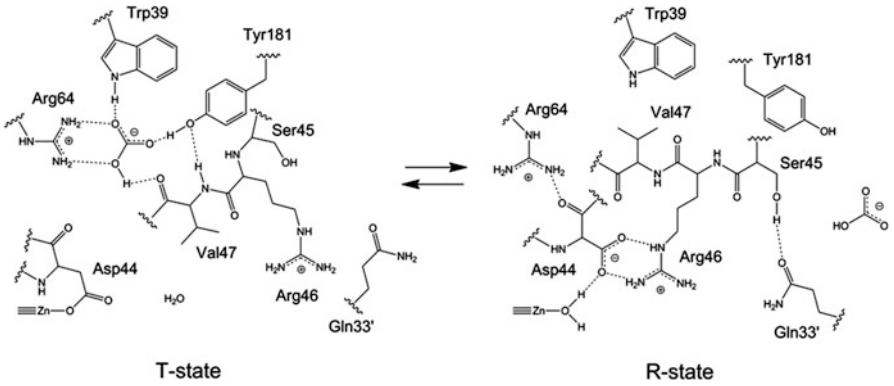

Fig. 4.6 Key residues involved in the allosteric switching of HICA between the inactive (T) and active (R) states

loss of 2 or 4 protons to generate the catalytically competent species [35]. Finally, the variation of both R_1 and R_{H2O} with $[CO_2 + HCO_3^-]$ concentration is biphasic: at low substrate concentration, these rates increase with increasing $[CO_2 + HCO_3^-]$ concentration; at higher $[CO_2 + HCO_3^-]$ concentrations R_1 and R_{H2O} decrease as the square of the $[CO_2 + HCO_3^-]$ concentration [35]. This data, when combined with the observation that bicarbonate ion binds to a non-catalytic site in HICA, suggests that HICA is an allosteric enzyme that is regulated by HCO_3^-, and that the fundamental allosteric unit is a dimer, presumably the fundamental structural dimer of β-CA. It seems likely that all type II β-CAs that have an intact Arg-Trp-Tyr triad in the non-catalytic pocket are likewise allosteric enzymes. The inactive T-state of type II β-CA is characterized by the vast majority of the X-ray crystallographic structures of the type II enzymes, where the active site Asp residue has displaced the catalytically essential water molecule. The active, R-state of the enzyme is assumed to closely resemble that of the type I β-CAs. The T-state of the enzyme is favored at low pH, when the metal-bound hydroxide is protonated to form a metal-bound water, which is more easily displaced than hydroxide by the side chain of the active site Asp residue. Figure 4.6 summarizes the principal elements of the T $\leftrightarrows$ R transition in HICA. Bicarbonate ion stabilizes the T-state by displacing the side chain of Val47 to interact with Trp39, Arg64, and Tyr181, as well as two water molecules and the carbonyl oxygen of Val47. Displacement of the polypeptide backbone from residues 44–48 disrupts the Asp44-Arg46 dyad, allowing Asp44 to coordinate to the metal ion. In the absence of HCO_3^-, Val47 can occupy its place and form a hydrophobic cluster with Trp39 and Tyr181, stabilizing the 44–48 loop in a way that allows for the formation of the Asp44-Arg46 dyad.

There is compelling evidence that type II β-CAs can adopt alternate conformations. The thiocyanate complex of Rv3588 crystallizes in an "R-state" conformation that resembles Type I β-CAs, whereas the uncomplexed enzyme crystallizes in a "T-state" conformation characteristic of Type II β-CAs. These structures suggest

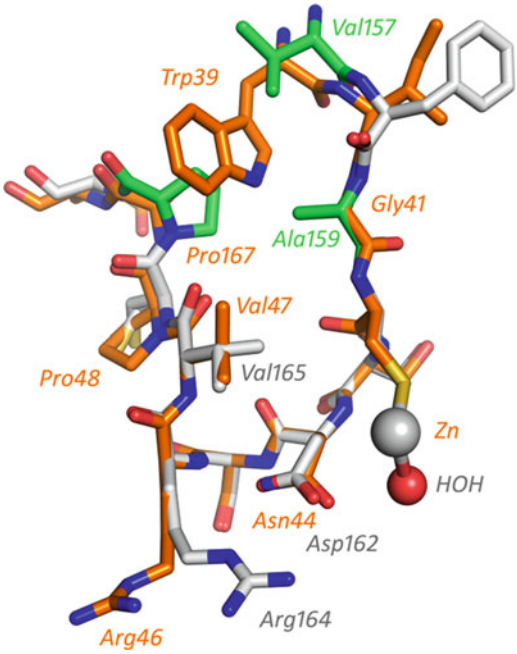

Fig. 4.7 Superposition of the allosteric loop region of HICA-D44N (PDB 3E1V, *orange backbone*) onto PSCA (PDB 1EKJ, *gray backbone*). HICA-D44N zinc ion and metal-bound water are depicted as *spheres*. *Green-backbone* residues indicate key structural differences in PSCA compared to HICA. HICA residues numbers are *orange*, PSCA *gray* or *green*

that Rv3588 can adopt two conformations in solutions that are distinguished by a "carboxylate shift" at the active site metal ion [39]. It is not known if HCO_3^- can bind to the noncatalytic site of Rv3588. Site-directed mutagenesis of HICA also supports the allosteric switching mechanism of Fig. 4.6. The allosteric site variant W39F retains a large fraction of the activity of the wild-type enzyme, but the apparent K_i for bicarbonate ion increases almost 5-fold for the variant enzyme [57]. This result is consistent with the loss of a stabilizing hydrogen bond for the binding of bicarbonate in the allosteric site.

The active site variant D44N, in which the active site Asp residue is replaced with an isosteric but non-nucleophilic Asn residue, is not active, but the critical 44–48 loop occupies precisely the same conformation (within 0.2 Å rmsd) as the analogous loop in the type I β-CA PSCA (Fig. 4.7) [57]. The observation of this structure in HICA-D44N suggests that (1) the enzyme can adopt more than one conformation about the active site, and (2) the stabilization of the "type I like" structure may be linked to the dissociation of the active site Asp from the metal ion. There are three key differences in the 39–50 loop (HICA numbering) between HICA and PSCA that may account for the former to adopt a bicarbonate-stabilized "T-state" while the latter cannot (Fig. 4.7). The first is the substitution of Ala for Gly41 in PSCA. This Ala residue pokes into the bicarbonate binding site, and would appear to preclude the binding of bicarbonate ion in the "T-state." The second is the substitution of Val for Trp39, which has been shown to significantly weaken bicarbonate binding to

the allosteric site [57]. Finally, a Pro residue that occupies position 48 in HICA is shifted one residue later in the sequence in PSCA. This proline shift has the effect of pointing the proline ring directly into the bicarbonate binding site. The G41A variant of HICA is essentially identical to wild-type, and is observed to bind bicarbonate ion in the allosteric site despite the steric hindrance predicted by the protruding methyl group of Ala [71]. This result suggests that the proline shift may be a critical factor in distinguishing allosteric and non-allosteric β-CAs. In PSCA, the region that would correspond to the allosteric site in HICA forms what looks like a stable hydrophobic cluster with the ring of Pro167, Val157, Ala159, and Val165, stabilizing the R-state conformation.

Direct evidence pH-cooperativity and bicarbonate-induced changes at the active site comes from spectroscopic studies of Co-HICA [61]. The *d-d* transitions in Co-HICA change significantly in both molar absorptivity and the wavelength of maximum absorption in a highly cooperative manner with a $[H^+]^4$ dependence, and an apparent pK_a near 7.8, which corresponds closely to the pK_a observed in the pH-rate profile of k_{cat}/K_m for CO_2 hydration. The low-pH spectrum is presumed to be due to the T-state of the enzyme, whereas the high-pH spectrum is believed to be representative of the R-state. Near but just above the transition point (pH 8.0), the addition of 25 mM HCO_3^- causes Co-HICA to switch from the high-pH spectrum to that essentially identical to the low-pH spectrum. This suggests that HCO_3^- can stabilize the T-state of the HICA. Remarkably, heterogeneously substituted Co-HICA (for which the principal absorbing species are Co-Zn heterodimers) and homogeneously substituted Co-HICA (for which the principal absorbing species are Co-Co dimers), are different colors. Partially Co-substituted Co-HICA is green, whereas homogeneous Co-HICA is blue. This easily observable qualitative color difference is due to the shift of a ligand-to-metal charge transfer band from 410 nm in the partially substituted enzyme into the UV tail for homogeneous Co-HICA. This strange result suggests that the metal ion in one active site of the fundamental dimer is coupled to and can be affected by the metal present in the other half of the dimer: that is, the fundamental dimer metal sites are cooperatively coupled.

The likely ingress/egress route for allosteric bicarbonate ion was serendipitously discovered in bicarbonate complexes of the allosteric site HICA variants G41A and V47A. In these variants, bicarbonate ion is observed to bind to a crevice along the dimerization interface between two Arg64 and two Glu50 residues. This site is immediately adjacent to the allosteric binding site, and has been designated the bicarbonate "escort" site [71]. A bicarbonate ion could easily transition between the "escort" site and the allosteric site by a relatively simple movement of one of the Arg64 residues. Indeed in the V47A variant, bicarbonate ions are observed to be bound in both allosteric sites and the "escort" site in the fundamental dimer. Sulfate, an apparent activator of HICA [35], is also observed to bind at the "escort" site, suggesting that the mode of activation could be related to blocking access of bicarbonate to the allosteric site [71].

6 Conclusion

The β-CAs are diverse in distribution in nature, and are one of five convergently evolved classes of CA that have arrived at the same, efficient solution for catalysis: a metal-hydroxide mechanism that is rate-limited by proton transfer. Uniquely, the β-CAs harbor the only known allosteric CAs. The role of significance of allostery in β-CA is not presently known.

Acknowledgments The author wishes to acknowledge the support of the National Science Foundation (MCB-0741396, MCB-1157332, and CHE0819686) for support of β-CA research at Colgate University.

References

1. Burnell JN, Gibbs MJ, Mason JG (1990) Spinach chloroplastic carbonic-anhydrase—nucleotide-sequence analysis of cDNA. Plant Physiol 92:37–40
2. Neish AC (1939) Chloroplasts. II. Their chemical composition and the distribution of certain metabolites between the chloroplasts and the remainder of the leaf. Biochem J 33:300–308
3. Coleman JR, Luinenburg I, Majeau N, Provart N (1991) Sequence analysis and regulation of expression of a gene coding for carbonic anhydrase in *Chlamydomonas reinhardtii*. Can J Bot 69:1097–1102
4. Roeske CA, Ogren WL (1990) Nucleotide sequence of pea cDNA-encoding chloroplast carbonic anhydrase. Nucleic Acids Res 18:3413
5. Moroney JV, Bartlett SG, Samuelsson G (2001) Carbonic anhydrases in plants and algae. Plant Cell Environ 24:141–153
6. Smith KS, Ferry JG (2000) Prokaryotic carbonic anhydrases. FEMS Microbiol Rev 24:335–366
7. Smith KS, Jakubzick C, Whittam TS, Ferry JG (1999) Carbonic anhydrase is an ancient enzyme widespread in prokaryotes. Proc Natl Acad Sci U S A 96:15184–15189
8. Rowlett RS (2010) Structure and catalytic mechanism of the beta-carbonic anhydrases. Biochim Biophys Acta Proteins Proteomics 1804:362–373
9. Nishimori I, Minakuchi T, Kohsaki T, Onishi S, Takeuchi H, Vullo D, Scozzafava A, Supuran CT (2007) Carbonic anhydrase inhibitors: the beta-carbonic anhydrase from *Helicobacter pylori* is a new target for sulfonamide and sulfamate inhibitors. Bioorg Med Chem Lett 17:3585–3594
10. Nishimori I, Minakuchi T, Vullo D, Scozzafava A, Supuran CT (2011) Inhibition studies of the β-carbonic anhydrases from the bacterial pathogen *Salmonella enterica* serovar Typhimurium with sulfonamides and sulfamates. Bioorg Med Chem 19:5023–5030
11. Joseph P, Ouahrani-Bettache S, Montero JL, Nishimori I, Minakuchi T, Vullo D, Scozzafava A, Winum JY, Kohler S, Supuran CT (2011) A new beta-carbonic anhydrase from *Brucella suis*, its cloning, characterization, and inhibition with sulfonamides and sulfamates, leading to impaired pathogen growth. Bioorg Med Chem 19:1172–1178
12. Burghout P, Vullo D, Scozzafava A, Hermans PWM, Supuran CT (2011) Inhibition of the beta-carbonic anhydrase from *Streptococcus pneumoniae* by inorganic anions and small molecules: toward innovative drug design of antiinfectives? Bioorg Med Chem 19:243–248
13. Smith KS, Ferry JG (1999) A plant-type (beta-class) carbonic anhydrase in the thermophilic methanoarchaeon *Methanobacterium thermoautotrophicum*. J Bacteriol 181:6247–6253

14. Amoroso G, Morell-Avrahov L, Muller D, Klug K, Sultemeyer D (2005) The gene NCE103 (YNL036w) from *Saccharomyces cerevisiae* encodes a functional carbonic anhydrase and its transcription is regulated by the concentration of inorganic carbon in the medium. Mol Microbiol 56:549–558
15. So AKC, Espie GS (1998) Cloning, characterization and expression of carbonic anhydrase from the cyanobacterium Synechocystis PCC6803. Plant Mol Biol 37:205–215
16. Sawaya MR, Cannon GC, Heinhorst S, Tanaka S, Williams EB, Yeates TO, Kerfeld CA (2006) The structure of beta-carbonic anhydrase from the carboxysomal shell reveals a distinct subclass with one active site for the price of two. J Biol Chem 281:7546–7555
17. Eriksson M, Karlsson J, Ramazanov Z, Gardestrom P, Samuelsson G (1996) Discovery of an algal mitochondrial carbonic anhydrase: molecular cloning and characterization of a low-CO_2-induced polypeptide in *Chlamydomonas reinhardtii*. Proc Natl Acad Sci U S A 93:12031–12034
18. Mitsuhashi S, Mizushima T, Yamashita E, Yamamoto M, Kumasaka T, Moriyama H, Ueki T, Miyachi S, Tsukihara T (2000) X-ray structure of beta-carbonic anhydrase from the red alga, *Porphyridium purpureum*, reveals a novel catalytic site for CO_2 hydration. J Biol Chem 275:5521–5526
19. Syrjanen L, Tolvanen M, Hilvo M, Olatubosun A, Innocenti A, Scozzafava A, Leppiniemi J, Niederhauser B, Hytonen VP, Gorr TA, Parkkila S, Supuran CT (2010) Characterization of the first beta-class carbonic anhydrase from an arthropod (*Drosophila melanogaster*) and phylogenetic analysis of beta-class carbonic anhydrases in invertebrates. BMC Biochem 11, No pp given
20. Fasseas MK, Tsikou D, Flemetakis E, Katinakis P (2010) Molecular and biochemical analysis of the β class carbonic anhydrases in *Caenorhabditis elegans*. Mol Biol Rep 37:2941–2950
21. Majeau N, Coleman JR (1996) Effect of CO_2 concentration on carbonic anhydrase and ribulose-1,5-bisphosphate carboxylase/oxygenase expression in pea. Plant Physiol 112:569–574
22. Majeau N, Arnoldo M, Coleman JR (1994) Modification of carbonic anhydrase activity by antisense and over-expression constructs in transgenic tobacco. Plant Mol Biol 25:377–385
23. Fukuzawa H, Suzuki E, Komukai Y, Miyachi S (1992) A gene homologous to chloroplast carbonic anhydrase (icfA) is essential to photosynthetic carbon dioxide fixation by Synechococcus PCC7942. Proc Natl Acad Sci U S A 89:4437–4441
24. Merlin C, Masters M, McAteer S, Coulson A (2003) Why is carbonic anhydrase essential to *Escherichia coli*? J Bacteriol 185:6415–6424
25. Mitsuhashi S, Ohnishi J, Hayashi M, Ikeda M (2004) A gene homologous to beta-type carbonic anhydrase is essential for the growth of *Corynebacterium glutamicum* under atmospheric conditions. Appl Microbiol Biotechnol 63:592–601
26. Gotz R, Gnann A, Zimmermann FK (1999) Deletion of the carbonic anhydrase-like gene NCE103 of the yeast *Saccharomyces cerevisiae* causes an oxygen-sensitive growth defect. Yeast 15:855–864
27. Clark D, Rowlett RS, Coleman JR, Klessig DF (2004) Complementation of the yeast deletion mutant Delta NCE103 by members of the beta class of carbonic anhydrases is dependent on carbonic anhydrase activity rather than on antioxidant activity. Biochem J 379:609–615
28. Burghout P, Cron LE, Gradstedt H, Quintero B, Simonetti E, Bijlsma JJE, Bootsma HJ, Hermans PWM (2010) Carbonic anhydrase is essential for *Streptococcus pneumoniae* growth in environmental ambient air. J Bacteriol 192:4054–4062
29. Bury-Mone S, Mendz GL, Ball GE, Thibonnier M, Stingl K, Ecobichon C, Ave P, Huerre M, Labigne A, Thiberge J-M, De RH (2008) Roles of α and β carbonic anhydrases of *Helicobacter pylori* in the urease-dependent response to acidity and in colonization of the murine gastric mucosa. Infect Immun 76:497–509
30. Smeulders MJ, Barends TRM, Pol A, Scherer A, Zandvoort MH, Udvarhelyi A, Khadem AF, Menzel A, Hermans J, Shoeman RL, Wessels HJCT, van den Heuvel LP, Russ L, Schlichting I, Jetten MSM, den Camp HJMO (2011) Evolution of a new enzyme for carbon disulphide conversion by an acidothermophilic archaeon. Nature (London, UK) 478:412–416

31. Kimber MS, Pai EF (2000) The active site architecture of *Pisum sativum* beta-carbonic anhydrase is a mirror image of that of alpha-carbonic anhydrases. EMBO J 19:1407–1418
32. Cronk JD, Endrizzi JA, Cronk MR, O'Neill JW, Zhang KYJ (2001) Crystal structure of *E-coli* beta-carbonic anhydrase, an enzyme with an unusual pH-dependent activity. Protein Sci 10:911–922
33. Krissinel E, Henrick K (2007) Inference of macromolecular assemblies from crystalline state. J Mol Biol 372:774–797
34. So AK, Espie GS, Williams EB, Shively JM, Heinhorst S, Cannon GC (2004) A novel evolutionary lineage of carbonic anhydrase (epsilon class) is a component of the carboxysome shell. J Bacteriol 186:623–630
35. Cronk JD, Rowlett RS, Zhang KYJ, Tu CK, Endrizzi JA, Lee J, Gareiss PC, Preiss JR (2006) Identification of a novel noncatalytic bicarbonate binding site in eubacterial beta-carbonic anhydrase. Biochemistry 45:4351–4361
36. Strop P, Smith KS, Iverson TM, Ferry JG, Rees DC (2001) Crystal structure of the "cab"-type beta class carbonic anhydrase from the archaeon *Methanobacterium thermoautotrophicum*. J Biol Chem 276:10299–10305
37. Smith KS, Cosper NJ, Stalhandske C, Scott RA, Ferry JG (2000) Structural and kinetic characterization of an archaeal beta-class carbonic anhydrase. J Bacteriol 182:6605–6613
38. Covarrubias AS, Larsson AM, Hogbom M, Lindberg J, Bergfors T, Bjorkelid C, Mowbray SL, Unge T, Jones TA (2005) Structure and function of carbonic anhydrases from *Mycobacterium tuberculosis*. J Biol Chem 280:18782–18789
39. Covarrubias AS, Bergfors T, Jones TA, Hoegbom M (2006) Structural mechanics of the pH-dependent activity of beta-carbonic anhydrase from *Mycobacterium tuberculosis*. J Biol Chem 281:4993–4999
40. Pocker Y, Ng JSY (1973) Plant carbonic anhydrase. Properties and carbon dioxide hydration kinetics. Biochemistry 12:5127–5134
41. Rowlett RS, Tu C, McKay MM, Preiss JR, Loomis RJ, Hicks KA, Marchione RJ, Strong JA, Donovan GS, Chamberlin JE (2002) Kinetic characterization of wild-type and proton transfer-impaired variants of beta-carbonic anhydrase from *Arabidopsis thaliana*. Arch Biochem Biophys 404:197–209
42. Majeau N, Coleman JR (1992) Nucleotide sequence of a complementary DNA encoding tobacco chloroplastic carbonic anhydrase. Plant Physiol 100:1077–1078
43. Raines CA, Horsnell PR, Holder C, Lloyd JC (1992) *Arabidopsis thaliana* carbonic anhydrase: cDNA sequence and effect of carbon dioxide on mRNA levels. Plant Mol Biol 20:1143–1148
44. Hoang CV, Wessler HG, Local A, Turley RB, Benjamin RC, Chapman KD (1999) Identification and expression of cotton (Gossypium hirsutum L.) plastidial carbonic anhydrase. Plant Cell Physiol 40:1262–1270
45. Johansson IM, Forsman C (1992) Processing of the chloroplast transit peptide of pea carbonic anhydrase in chloroplasts and in *Escherichia coli*: identification of 2 cleavage sites. FEBS Lett 314:232–236
46. Forsman C, Pilon M (1995) Chloroplast import and sequential maturation of pea carbonic anhydrase: the roles of various parts of the transit peptide. FEBS Lett 358:39–42
47. Rowlett RS, Chance MR, Wirt MD, Sidelinger DE, Royal JR, Woodroffe M, Wang Y-FA, Saha RP, Lam MG (1994) Kinetic and structural characterization of spinach carbonic anhydrase. Biochemistry 33:13967–13976
48. Johansson IM, Forsman C (1993) Kinetic studies of pea carbonic anhydrase. Eur J Biochem 218:439–446
49. Johansson IM, Forsman C (1994) Solvent hydrogen isotope effects and anion inhibition of CO_2 hydration catalysed by carbonic anhydrase from *Pisum sativum*. Eur J Biochem 224:901–907
50. Smith KS, Ingram-Smith C, Ferry JG (2002) Roles of the conserved aspartate and arginine in the catalytic mechanism of an archaeal beta-class carbonic anhydrase. J Bacteriol 184:4240–4245

51. Innocenti A, Hall RA, Schlicker C, Muhlschlegel FA, Supuran CT (2009) Carbonic anhydrase inhibitors. Inhibition of the beta-class enzymes from the fungal pathogens *Candida albicans* and *Cryptococcus neoformans* with aliphatic and aromatic carboxylates. Bioorg Med Chem 17:2654–2657
52. Domsic JF, Avvaru BS, Kim CU, Gruner SM, Agbandje-McKenna M, Silverman DN, McKenna R (2008) Entrapment of carbon dioxide in the active site of carbonic anhydrase II. J Biol Chem 283:30766–30771
53. Bjorkbacka H, Johansson IM, Forsman C (1999) Possible roles for His 208 in the active-site region of chloroplast carbonic anhydrase from *Pisum sativum*. Arch Biochem Biophys 361:17–24
54. Rowlett RS, Tu C, Murray PS, Chamberlin JE (2004) Examination of the role of Gln-158 in the mechanism of CO_2 hydration catalyzed by beta-carbonic anhydrase from *Arabidopsis thaliana*. Arch Biochem Biophys 425:25–32
55. Hakkim V, Rajapandian V, Subramanian V (2011) Density functional theory investigations of the catalytic mechanism of β-carbonic anhydrase. Indian J Chem A Inorg Bio-inorg Phys Theor Anal Chem 50A:503–510
56. Provart NJ, Majeau N, Coleman JR (1993) Characterization of pea chloroplastic carbonic anhydrase—expression in *Escherichia coli* and site-directed mutagenesis. Plant Mol Biol 22:937–943
57. Rowlett RS, Tu C, Lee J, Herman AG, Chapnick DA, Shah SH, Gareiss PC (2009) Allosteric site variants of *Haemophilus influenzae* beta-carbonic anhydrase. Biochemistry 48:6146–6156
58. Silverman DN, Lindskog S (1988) The catalytic mechanism of carbonic anhydrase: implications of a rate-limiting protolysis of water. Acc Chem Res 21:30–36
59. Tripp BC, Ferry JG (2000) A structure-function study of a proton transport pathway in the gamma-class carbonic anhydrase from *Methanosarcina thermophila*. Biochemistry 39:9232–9240
60. Tu CK, Rowlett RS, Tripp BC, Ferry JG, Silverman DN (2002) Chemical rescue of proton transfer in catalysis by carbonic anhydrases in the beta- and gamma-class. Biochemistry 41:15429–15435
61. Hoffmann KM, Samardzic D, Heever K, Rowlett RS (2011) Co(II)-substituted *Haemophilus influenzae* beta-carbonic anhydrase: spectral evidence for allosteric regulation by pH and bicarbonate ion. Arch Biochem Biophys 511:80–87
62. Pocker Y, Ng JSY (1974) Plant carbonic anhydrase. Hydrase activity and its reversible inhibition. Biochemistry 13:5116–5120
63. Zimmerman S, Innocenti A, Casini A, Ferry JG, Scozzafava A, Supuran CT (2004) Carbonic anhydrase inhibitors. Inhibition of the prokaryotic beta- and gamma-class enzymes from Archaea with sulfonamides. Bioorg Med Chem Lett 14:6001–6006
64. Zimmerman SA, Ferry JG, Supuran CT (2007) Inhibition of the archaeal beta-class (Cab) and gamma-class (Cam) carbonic anhydrases. Curr Top Med Chem 7:901–908
65. Isik S, Kockar F, Arslan O, Guler OO, Innocenti A, Supuran CT (2008) Carbonic anhydrase inhibitors. Inhibition of the beta-class enzyme from the yeast *Saccharomyces cerevisiae* with anions. Bioorg Med Chem Lett 18:6327–6331
66. Isik S, Kockar F, Aydin M, Arslan O, Guler OO, Innocenti A, Scozzafava A, Supuran CT (2009) Carbonic anhydrase inhibitors: inhibition of the beta-class enzyme from the yeast *Saccharomyces cerevisiae* with sulfonamides and sulfamates. Bioorg Med Chem 17:1158–1163
67. Morishita S, Nishimori I, Minakuchi T, Onishi S, Takeuchi H, Sugiura T, Vullo D, Scozzafava A, Supuran CT (2008) Cloning, polymorphism, and inhibition of beta-carbonic anhydrase of *Helicobacter pylori*. J Gastroenterol 43:849–857
68. Innocenti A, Muhlschlegel FA, Hall RA, Steegborn C, Scozzafava A, Supuran CT (2008) Carbonic anhydrase inhibitors: inhibition of the beta-class enzymes from the fungal pathogens *Candida albicans* and *Cryptococcus neoformans* with simple anions. Bioorg Med Chem Lett 18:5066–5070

69. Lindskog S (1969) Mechanism of sulfonamide inhibition of carbonic anhydrase. Chalmers Institute and University of Technology, Goteborg, Sweden, pp 157–165
70. Innocenti A, Zimmerman S, Ferry JG, Scozzafava A, Supuran CT (2004) Carbonic anhydrase inhibitors. Inhibition of the beta-class enzyme from the methanoarchaeon *Methanobacterium thermoautotrophicum* (Cab) with anions. Bioorg Med Chem Lett 14:4563–4567
71. Rowlett RS, Hoffmann KM, Failing H, Mysliwiec MM, Samardzic D (2010) Evidence for a bicarbonate "escort" site in *Haemophilus influenzae* beta-carbonic anhydrase. Biochemistry 49:3640–3647